ISBN: 978-3-95450-227-1 ISSN: 2673-5490 doi:10.18429/JACoW-IPAC2022-THPOPT017

ORBIT STABILITY STUDIES FOR THE DIAMOND-II STORAGE RING

I.P.S. Martin, C.A. Abraham, D. Crivelli, H. Ghasem, B. Nicholson, T. Olsson, P. Sanchez-Navarro,
Diamond Light Source, Oxfordshire, U.K.

Abstract

The photon-beam stability relative to the beam size is a key performance parameter for storage ring light sources. The natural emittance of the Diamond-II ring will be lowered by a factor 16.7 compared to the existing facility [1], so the absolute stability requirement for the electron beam must reduce accordingly. In addition, advances in detector speed and resolution mean the tolerances are tighter compared to previous generations of storage rings, with a target of 3 % of beam size up to 1 kHz having been adopted for Diamond-II. In this paper we present studies of how the anticipated ground vibrations, girder motion, power supply ripple and RF noise will affect the electron beam stability as a function of frequency.

INTRODUCTION

To cope with advances in beamline detector speed and resolution, the target electron beam stability has been increased from 10% of beam size in the range 1-100 Hz for Diamond to 3% in the 1-1000 Hz bandwidth for Diamond-II. The new storage ring has an emittance of 162 pm.rad, corresponding to a factor ~5 reduction in horizontal beam size at the centre of the straights compared to the existing machine [1]. The vertical beam sizes at the source points are largely unchanged, as for both machines the β-functions are similar and the vertical emittance has been fixed at 8 pm.rad.

The increased stability requirements place strong demands on the facility design. To relieve the demands on the fast orbit feedback system, the storage ring components are being designed with their impact on electron beam stability considered from an early stage. Within the target bandwidth, the major contributors are expected to be ground vibrations, girder resonances, power supply ripple and RF noise. This paper contains a first analysis of how each of these sources are expected to contribute to the underlying electron beam stability. The target stability values for Diamond-II are given in Table 1.

Table 1: Required Electron Beam Stability (r.m.s.)

Location	Horizontal	Vertical
Long Straight	1.08 μm	0.16 μm
Standard Straight	0.87 μm	0.13 μm
Mid Straight	0.83 μm	0.11 μm

SOURCES OF DISTURBANCE

Ground Motion

Ground vibrations have been measured in the range 0.02 to 250 Hz using a combination of a Guralp seismometer and PCB seismic accelerometers [2]. In addition to the amplitude, the phase correlation of the ground motion has been measured along the vertical and North-South axes using two seismic accelerometers connected by a >100 m long cable [3]. The separation of the accelerometers was increased in steps and at each separation the amplitude and phase of the ground motion was recorded. This data was then used to extract the frequency at which the measured vibrations switch from being coherent to incoherent: motion with a phase deviation of below 45 degrees was defined to be in-phase (i.e. correlated) and anything greater than this was taken to be uncorrelated. Results are shown in Fig. 1.

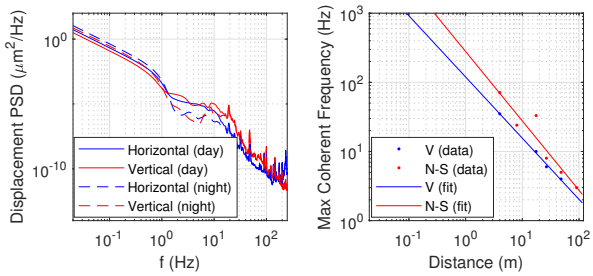

Figure 1: Left: Displacement power spectral density (PSD) for the Diamond tunnel. Right: Cross-over frequency when moving from correlated to uncorrelated motion.

An exponential fit was made to the correlation data to extract the general trend. The approximate scaling in each plane was found to be:

$$L_{coh,V} \approx \frac{222}{f^{1.1}}, \qquad L_{coh,N-S} \approx \frac{273}{f^{1.0}}. \tag{1}$$

From this analysis, for distances of up to ~10 m (corresponding to the length of a single girder or the BPM separation across an ID straight section), vibrations travelling through the storage ring floor will be coherent at frequencies up to around 15-25 Hz. That is to say, motion at these frequencies will be in-phase and everything supported by the slab will move as a single body.

The impact that ground motion has on electron beam stability has been analysed following a similar method to that described in [4]. Random displacements were calculated for the storage ring magnets over 100 seeds for a given correlation length. Ground-displacement to electron beam amplification factors could then be derived for each case by dividing the RMS closed orbit distortion at the source points by the amplitude of the ground motion and then averaging over the 100 seeds [1]. The results for that correlation length were then converted to excitation frequency using Eq. 1. Examples of the generated ground displacement for two correlation lengths are shown in Fig. 2.

ISBN: 978-3-95450-227-1 ISSN: 2673-5490 doi:10.18429/JACoW-IPAC2022-THPOPT017

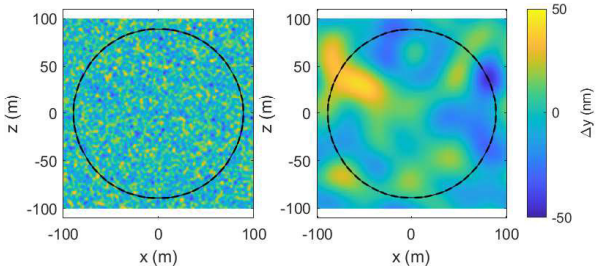

Figure 2: Vertical ground displacement for a single seed with a correlation length of 5 m (left) and 50 m (right).

The girder structures will exhibit resonances at particular frequencies. Finite element analysis (FEA) has been conducted on the combined storage ring tunnel / girder structure to investigate the behaviour in the frequency range from 5 Hz to 120 Hz. This showed the dominant motion of the magnets derives from displacement of the tunnel floor, rather than resonances in the girder structure itself. This results from the girder having a high degree of stiffness thanks to it being constrained by five separate pedestals along its length.

Ground-to-electron beam amplification factors due to girder resonances were again calculated by simulating 100 random machines at different excitation frequencies, with each girder distorted according to the FEA mode-shapes and with uncorrelated oscillation phase offsets. An amplification factor was found for each frequency by dividing the closed orbit amplitude at the source points by the displacement used in the FEA simulations. Results are shown in Fig. 3.

An overall amplification factor was calculated by combining the contributions from ground motion and girder resonances. This was then used to calculate the expected electron beam motion due to ground vibrations, the results of which are shown in Fig. 4. The integrated electron beam motion in the frequency range 0.02-250 Hz at the centre of a standard straight was found to be 51 nm horizontally and 114 nm vertically.

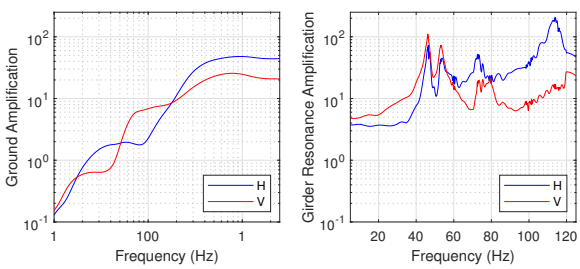

Figure 3: Amplification factors due to coherent displacements (left) and girder resonances (right).

Power Supply Ripple

As the Diamond-II power supplies are not yet available, the existing DDBA magnet power supplies were used to estimate the noise in the 0.1-1000 Hz band. The impact on the electron beam was estimated using the following procedure:

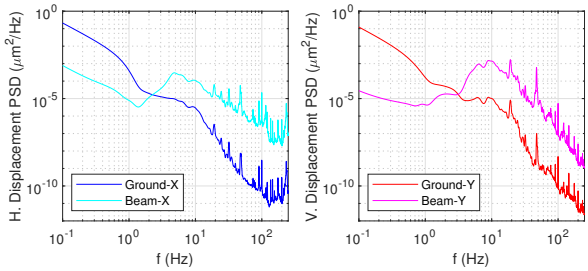

Figure 4: Simulated electron beam displacement in the standard straights compared to measured ground motion.

1. extract a calibration factor (Amps to field) from each of the OPERA magnet models;
2. calculate frequency-dependent attenuation factors for the relevant vacuum chambers and solid-core magnets;
3. create 50 random machine models using the Simulated Commissioning process [5];
4. apply uncorrelated field errors to all the magnets of each type and calculate the change in closed orbit;
5. average the results across the 50 seeds and use the calibration factors to get a power supply amplification factor for each magnet;
6. Multiply the power supply PSD by the square of the amplification and attenuation factors to get the electron beam displacement.

The vacuum-chamber attenuation factors were calculated assuming circular cross-section vacuum pipes of 10 mm inner radius using the theory described in [6]. Additional attenuation factors for the solid-core magnets (the DQ dipoles and the anti-bends) were calculated using the OPERA magnet model.

The electron beam PSDs due to power supply ripple calculated using this method are shown in Fig. 5. Despite the additional attenuation coming from the solid yokes, the largest contribution to horizontal electron beam motion comes from the DQ gradient dipoles and the anti-bend quadrupoles. In the vertical plane it is the noise on the vertical steerers that dominates. The integrated values in the 0.14-1000 Hz bandwidth are summarised in Table 2.

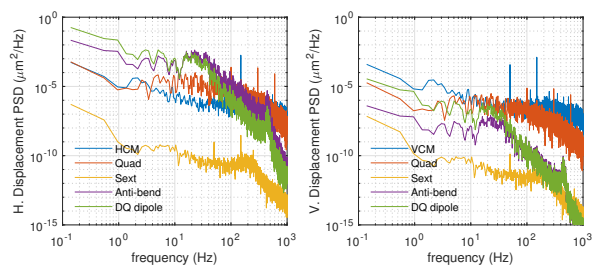

Figure 5: Electron beam motion due to power supply ripple.

Energy Variation

The primary source of energy variation is expected to be noise on the RF voltage and phase. This has been simulated by tracking 1 million particles in ELEGANT [7] using a one-

ISBN: 978-3-95450-227-1 ISSN: 2673-5490 doi:10.18429/JACoW-IPAC2022-THPOPT017

Table 2: Integrated Electron Beam Motion in the 0.14-1000 Hz Bandwidth Due to Power Supply Ripple

Magnet Type	# Magnets	Total H	Total V
Corrector	252	49 nm	41 nm
Quadrupole	300	57 nm	10 nm
Sextupole	288	0.5 nm	0.2 nm
Anti-bend	96	254 nm	1.1 nm
Gradient bend	48	367 nm	5.1 nm

turn map including radiation damping, quantum excitation and IDs. The RF noise has been included by applying uncorrelated Gaussian errors on each of the 8 main cavities with a standard deviation of 0.1% for the amplitude and 0.1 degrees for the phase, corresponding to the low-level RF specification. A passive super-conducting harmonic cavity has also been included in the simulation. This has been modelled as an ideal cavity with the voltage and phase set according to the flat potential conditions, without noise. Figure 6 shows the resulting electron beam displacement PSDs, with and without the harmonic cavity. The RF noise gives rise to an energy oscillation which translates into horizontal motion through the dispersion. The horizontal motion is therefore largest at the mid-straights. The results also show that the harmonic cavity broadens the peak of the synchrotron motion and moves it towards lower frequencies.

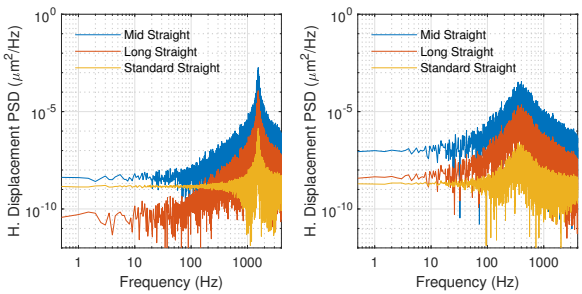

Figure 6: Horizontal PSDs for the lattice without (left) and with (right) harmonic cavity. Uncorrelated RF noise with 0.1% amplitude and 0.1 deg (1 σ) has been applied to each of the 8 main cavities.

The integrated horizontal displacement due to RF noise in the range 0.5-1000 Hz is given in Table 3. The harmonic cavity increases the total oscillation in the frequency range because of the shift of the synchrotron frequency towards lower frequencies, however, the overall contribution from RF remains small.

Total Electron Beam Motion

Estimates for the total electron beam PSDs have been created for each plane by combining the individual contributions in quadrature. In the horizontal plane the contributions from the RF and harmonic cavities have been included, and in all cases the amplitudes have been calculated for the centre of the standard straights (β_x = 5.5 m and β_y = 2.3 m). Results are shown in Fig. 7. The calculated rms displacement in the frequency range 0.1-1000 Hz is 411 nm horizontally and 121 nm vertically, corresponding to 1.4 % and 2.8 % of beam size respectively.

Table 3: Integrated Horizontal Displacement Due to RF Noise, With and Without Harmonic Cavity

Location	Without HC	With HC
Long Straight	4 nm	33 nm
Standard Straight	1 nm	4 nm
Mid Straight	15 nm	132 nm

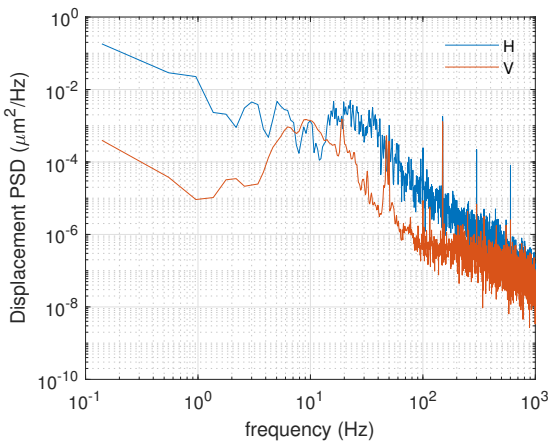

Figure 7: Expected electron beam PSDs at the centre of a standard straight including ground vibrations, girder resonances, power supply ripple and RF noise.

CONCLUSIONS

An analysis has been given of the expected electron beam stability for Diamond-II, including contributions from ground motion, girder resonances, power supply ripple and RF noise. Additional sources may exist which have not been included here, for example the cooling water flow, fast ID motion or injection pulsed magnets. However, the studies performed so far indicate the target electron beam stability for Diamond-II can be reached, even without the additional suppression coming from the fast orbit feedback.

Further studies on this topic are planned. A prototype girder has been delivered to Diamond, meaning it will soon be possible to replace the FEA data with measured vibrations. Actual magnet field variation due to power supply ripple should also be available, once the prototype magnets and power supplies have been delivered. Validation of the calculation methods presented here using the existing storage ring magnets are also planned.

REFERENCES

[1] "Diamond-II Conceptual Design Report", Diamond Light Source, 2019, https://www.diamond.ac.uk/Home/About/Vision/Diamond-II.html

ISBN: 978-3-95450-227-1 ISSN: 2673-5490 doi:10.18429/JACoW-IPAC2022-THPOPT017

[2] D. Crivelli, "Long Period, High Resolution Vibration Measurements of the Storage Ring Floor", Diamond-II internal note MENG-VIB-REP-220, 2021.

[3] D. Crivelli, T. Thomas, J. Poynton, "Frequency-Dependent Coherence of the Storage Ring Slab", Diamond-II internal note MENG-VIB-REP-221, 2021.

[4] V. Sajaev, C. Preissner, "Determination of the Ground Motion Orbit Amplification Factors Dependence on the Frequency for the APS Upgrade Storage Ring", in *Proc. IPAC'18, Vancouver*, Canada, Apr.-May 2018, pp. 1272-1275. doi:10.18429/JACoW-IPAC2018-TUPMF012

[5] H.-C. Chao, R.T. Fielder, J. Kallestrup, I.P.S. Martin, B. Singh, "Commissioning Simulations for the Diamond-II Upgrade", in *Proc. IPAC'22*, Bangkok, Thailand, June 2022, paper ID THPOPT016, this conference.

[6] B. Podobedov, L. Ecker, D. Harder, G. Rakowsky, "Eddy Current Shielding by Ellectically Thick Vacuum Chambers", in *Proc. PAC'09*, Vancouver, Canada, paper ID TH5PFP083, 2009.

[7] M. Borland, "elegant: a flexible sdds-compliant code for accelerator simulation", Advanced Photon Source, Argonne National Laboratory, USA, Report No. LS-287, 2000.